Toxicology and Applied Pharmacology 253 (2011) 81–93

Contents lists available at ScienceDirect

Toxicology and Applied Pharmacology

journal homepage: www.elsevier.com/locate/ytaap

Efficient internalization of silica-coated iron oxide nanoparticles of different sizes by primary human macrophages and dendritic cells

Andrea Kunzmann [a,1], Britta Andersson [b,1], Carmen Vogt [c], Neus Feliu [a], Fei Ye [c], Susanne Gabrielsson [b], Muhammet S. Toprak [c], Tina Buerki-Thurnherr [d], Sophie Laurent [e], Marie Vahter [f], Harald Krug [d], Mamoun Muhammed [c], Annika Scheynius [b], Bengt Fadeel [a,*]

[a] Division of Molecular Toxicology, Institute of Environmental Medicine, Karolinska Institutet, Stockholm, Sweden
[b] Clinical Allergy Research Unit, Department of Medicine Solna, Karolinska Institutet, Stockholm, Sweden
[c] Functional Materials Division, School of Information and Communication Technology, Royal Institute of Technology, Stockholm, Sweden
[d] Laboratory for Materials, Biology Interactions, Swiss Federal Laboratories of Materials Testing and Research, St. Gallen, Switzerland
[e] NMR and Molecular Imaging Laboratory, Department of General, Organic and Biomedical Chemistry, University of Mons, Mons, Belgium
[f] Division of Metals and Health, Institute of Environmental Medicine, Karolinska Institutet, Stockholm, Sweden

ARTICLE INFO

Article history:
Received 7 November 2010
Revised 4 March 2011
Accepted 14 March 2011
Available online 22 March 2011

Keywords:
Superparamagnetic nanoparticles
Surface coating
Biocompatibility
Cytokine secretion
Macrophages
Dendritic cells

ABSTRACT

Engineered nanoparticles are being considered for a wide range of biomedical applications, from magnetic resonance imaging to "smart" drug delivery systems. The development of novel nanomaterials for biomedical applications must be accompanied by careful scrutiny of their biocompatibility. In this regard, particular attention should be paid to the possible interactions between nanoparticles and cells of the immune system, our primary defense system against foreign invasion. On the other hand, labeling of immune cells serves as an ideal tool for visualization, diagnosis or treatment of inflammatory processes, which requires the efficient internalization of the nanoparticles into the cells of interest. Here, we compare novel monodispersed silica-coated iron oxide nanoparticles with commercially available dextran-coated iron oxide nanoparticles. The silica-coated iron oxide nanoparticles displayed excellent magnetic properties. Furthermore, they were non-toxic to primary human monocyte-derived macrophages at all doses tested whereas dose-dependent toxicity of the smaller silica-coated nanoparticles (30 nm and 50 nm) was observed for primary monocyte-derived dendritic cells, but not for the similarly small dextran-coated iron oxide nanoparticles. No macrophage or dendritic cell secretion of pro-inflammatory cytokines was observed upon administration of nanoparticles. The silica-coated iron oxide nanoparticles were taken up to a significantly higher degree when compared to the dextran-coated nanoparticles, irrespective of size. Cellular internalization of the silica-coated nanoparticles was through an active, actin cytoskeleton-dependent process. We conclude that these novel silica-coated iron oxide nanoparticles are promising materials for medical imaging, cell tracking and other biomedical applications.

Introduction

Magnetic nanoparticles are a widely studied class of nanoparticles as they offer great possibilities in a number of diagnostic applications and therapies (Laurent et al., 2009; Veiseh et al., 2009). In recent years, a new generation of nanoparticles with complex structures has emerged, carrying different functionalities which allow for the achievement of multiple tasks simultaneously, e.g. combined imaging and delivery of drugs to specific target organs (Riehemann et al., 2009). The core–shell architecture offers an attractive platform for development of multifunctional nanoparticles. The visualization function (i.e. for MRI applications) is performed via the core while the protective shell can be used for surface modification e.g. for targeted drug delivery (Salgueiriño-Maceira and Correa-Duarte, 2007; Kunzmann et al., 2011).

The MRI technique without the use of contrast agents has a limited sensitivity as well as a low resolution giving insufficient pathological information. The use of superparamagnetic iron oxide nanoparticle (SPION) based MRI contrast agents is well established and a number of SPIONs are approved by the U.S. Food and Drug Administration (FDA) (Hamm et al., 1994; Reimer and Balzer, 2003). For biomedical applications it is crucial that SPIONs have a well-defined shape, are monodisperse, and exhibit a high magnetization value (Laurent et al., 2009). However, SPIONs cannot be used as prepared, the agglomeration at physiological pH (Lu et al., 2007) and the rapid clearance from

* Corresponding author at: Division of Molecular Toxicology, Institute of Environmental Medicine, Karolinska Institutet, Nobels väg 13, S-171 77 Stockholm, Sweden. Fax: +46 8 34 38 49.
E-mail address: bengt.fadeel@ki.se (B. Fadeel).
[1] These authors have contributed equally.

0041-008X/$ – see front matter © 2011 Elsevier Inc. All rights reserved.
doi:10.1016/j.taap.2011.03.011

the blood being important drawbacks. Coating with an additional biocompatible layer such as dextran (Dutz et al., 2007), polyethylene glycol (Barrera et al., 2009) or silica (Bumb et al., 2008) is one of the common strategies to avoid these problems. Silica offers an inert coating material, preventing the aggregation of the superparamagnetic core in liquid media and enhancing their chemical stability. Furthermore, silica is a versatile material for surface modification which opens to new possibilities for the synthesis of nanoparticles for combined diagnostics and therapy (Liong et al., 2008; Bumb et al., 2010).

Among various methods of coating the iron oxide nanoparticles with silica the most common routes are the Stöber method (Stöber et al., 1968; Lu et al., 2002; Deng et al., 2005; Im et al., 2005) and the microemulsion process (Santra et al., 2001; Lu et al., 2007). The Stöber method, mainly used for synthesis of silica particles, is also applied for obtaining core–shell nanoparticles (Rao et al., 2005). Even though this method is technically simple, the core–shell nanoparticles are multicore and highly polydisperse, which limits their use for biomedical applications. The water-in-oil microemulsion (w/o), or inverse microemulsion, is a preferred method for the synthesis of monodisperse silica shell–magnetic core nanoparticles (Yi et al., 2005, 2006; Lu et al., 2007; Zhang et al., 2008; Narita et al., 2009). Even if the initially synthesized particles are uniform in size and shape, due to the residual condensation reaction during the washing steps, the final particles are strongly necked, aggregated and often multicore nanoparticles. These characteristics will result in the increase of the overall size, decreased surface area and reduced colloidal stability, which will hinder their potential use for *in vitro* or *in vivo* applications that require small size, high monodispersity and non-aggregated nanoparticles.

To promote a safe use of nanomaterials in biomedical applications, the cellular interactions of nanoparticles have to be carefully addressed (Kunzmann et al., 2011; Shvedova et al., 2010). At the same time, potential consequences for the immune system are important to consider (Dobrovolskaia and McNeil, 2007). Macrophages and dendritic cells are key players in the immune system (Banchereau and Steinman, 1998; Gordon and Taylor, 2005), and the use of primary human monocyte derived macrophages (HMDM) and dendritic cells (MDDC) is more relevant in *in vitro* model systems compared to the transformed cell lines that are commonly used in toxicity studies. Furthermore, when nanoparticles are applied in the clinical setting, it has to be ensured that the macrophage function is not impaired (Witasp et al., 2009b) and that dendritic cells are not activated to induce adverse immune reactions (Vallhov et al., 2006).

In order to use SPIONs as MRI agent, they have to be efficiently internalized by target cells. Targeting of immune cells facilitates diagnostic imaging, and with combined features such as tumor antigen loading (de Vries et al., 2005), therapeutic effects could be enhanced. Nowadays, MRI agents are used for a number of different applications. Macrophages are mainly involved in nonspecific uptake of particles and cellular debris. Thus, besides the classical liver imaging, MRI agents offer the possibility to track macrophages *in vivo*, allowing e.g. the depiction of immune responses (Fleige et al., 2002) and further permit a deeper insight into the process of diseases or pathologies (Flogel et al., 2008). In addition, when SPIONs are internalized by dendritic cells, MRI serves as an ideal tool for detecting migration of dendritic cells, offering the possibility to achieve an optimal immunotherapy (de Vries et al., 2005; Kobukai et al., 2010). Labeling of immune-competent cells with SPIONs enables the visualization of specific tissues with enrichment of such cells, which is relevant in e.g. cancer therapy (Valable et al., 2008).

With the aim to generate nanomaterials with improved performance for imaging applications as MRI and cell tracking, we synthesized different sized superparamagnetic silica-coated iron oxide nanoparticles, referred to as core–shell nanoparticles (CSNPs). We compared these to dextran-coated iron oxide nanoparticles (nanomag®-D-spio) commercially available and similar to clinically used SPIONs. The CSNPs were shown to display superior relaxivity values compared to the commercial nanoparticles, and good biocompatibility when incubated *in vitro* with primary human immune-competent cells, although some dose-dependent toxicity of the smaller silica-coated nanoparticles was recorded for primary human dendritic cells. Cellular internalization of the particles was shown to be active (actin cytoskeleton-dependent), and the degree of particle internalization by primary human macrophages appeared to depend on the surface coating, with significantly higher uptake of CSNPs compared to nanomag®-D-spio.

Materials and methods

Chemicals. Nanomag®-D-spio was purchased from Micromod Partikeltechnologie GmbH (Rostock-Warnemuende, Germany). Iron oxyhydroxide, FeO(OH) (30–50 mesh), Triton-X100 (analytical grade), cyclohexane (99.5%) and hexanol (98%) were purchased from Sigma Aldrich (St. Louis, MO) and oleic acid, tetraethyl orthosilicate (TEOS) (99.5%) and NH_4OH (28%) from Fluka (Sigma Aldrich). All chemicals were used as received. Ethanol was of 99.9% purity and the water was MilliQ grade with a resistivity of 18 MΩ.

Synthesis of silica-coated iron oxide nanoparticles (CSNPs). The synthesis of iron oxide core nanoparticles (with overall diameter of 30 nm and 50 nm) was done by a modified one-pot synthesis method (Lin et al., 2006). In a typical synthesis 2 mmol of iron oxyhydroxide and 8 mmol of oleic acid were heated to 320 °C for 45 min. The obtained oleic acid capped particles were separated by several cycles of precipitation with ethanol and dispersion in cyclohexane. The core particles were subsequently coated with a silica shell using an inverse microemulsion method (Triton X100/hexanol/water/cyclohexane system) as previously described (Vogt et al., 2010). Briefly, the SPION cyclohexane suspension (0.1 mg/mL Fe_3O_4) was mixed with Triton-X100, hexanol, H_2O and NH_4OH. TEOS was added and the stirring was continued for 2 h. CSNPs were obtained by combining the pH adjustment of the water phase of the microemulsion with rapid cooling in liquid N_2 and centrifugation at high rpm with subsequent redispersion in ethanol. To obtain particles with an average diameter of 120 nm and 70 nm (the control particles), the Stöber method was used (Stöber et al., 1968). In a typical experiment water and ethanol in a ratio of 2:3 were mixed with silica coated iron oxide particles with an overall diameter of 30 nm obtained as described above. The pH of the reaction was adjusted to 8–9 with NH_4OH. The condensation time was fixed to 2 h whereas the thickness of silica layer was tailored by adjusting the volume of TEOS. The particles were washed in water by several ultra-centrifugations at 2 °C and dispersed in water for further use.

Inductively coupled plasma-optical emission spectrometry (ICP-OES). A known volume of CSNPs was dispersed in water and the concentration of Fe and Si was measured in triplicate using an ICP Emission Spectrometer, iCAP 6000 series (Thermo Scientific, Waltham, United States). Fe and Si Accu Trace™ Reference Standard solutions for ICP (Analytical Standards AB, Mölnlycke, Sweden) were used.

Transmission electron microscopy (TEM). A drop of iron oxide particle suspension was air dried onto a carbon film coated TEM grid and analysis of nanoparticle size and morphology was performed using a JEM-2100 (JEOL Ltd., Tokyo, Japan) at 200 kV acceleration. The mean size diameter and SD were calculated after measuring at least 300 nanoparticles in random fields of view on the TEM micrographs.

Dynamic light scattering (DLS). The hydrodynamic diameter of the CSNPs and nanomag®-D-spio was measured using Malvern, Zetasizer

Nano ZS system (Malvern Instruments Ltd., Worcestershire, UK). The measurements were performed in deionized (DI) water (pH 7.0) at room temperature and after incubating the particles at 37 °C in RPMI 1640 cell culture media supplemented with 10% FCS (pH 7.4).

Zeta potential measurements. The effective charge on CSNPs and nanomag®-D-spio was measured using Beckman-Coulter DelsaNanoC system in the pH range of 4 to 9. pH titrations were performed using 0.1 M HCl and 0.1 M NaOH solutions in the auto-titrator unit.

Vibrating sample magnetometry (VSM). The magnetization measurements were performed using a vibrating sample magnetometer, VSM (Molspin Ltd., New Castle Upon Tyne, UK) in the magnetic field range of ±1 T.

Magnetic resonance (MR) relaxometry measurements. Longitudinal (r_1) and transverse (r_2) relaxivity measurements at 0.47 T and 1.41 T were obtained on Minispec MQ 20 and MQ 60 spin analyzers (Bruker, Karlsruhe, Germany). The measurements were performed on 300 μL of aqueous particle suspension with concentrations in the range of 2–7 mM/L Fe.

Endotoxin assay. Each batch of nanoparticles was controlled for lipopolysaccharide (LPS) contamination by using the chromogenic LAL test method (Limulus Amebocyte Lysate endochrome, Charles River Endosafe, Charleston, SC, USA) (Vallhov et al., 2006). The LPS levels were always below 50 pg/mL.

Generation of HMDM and MDDC. Peripheral blood mononuclear cells (PBMC) were prepared from buffy coats obtained from healthy blood donors (Karolinska University Hospital, Stockholm, Sweden) by density gradient centrifugation using Lymphoprep (Axis-Shield, Oslo, Norway) or Ficoll-Pacque PLUS (GE Healthcare Bio-Science AB) for human monocyte-derived macrophages (HMDM) or monocyte-derived dendritic cells (MDDC), respectively. Thereafter the PBMC were positively selected for CD14 expression (CD14 MicroBeads, human (Miltenyi Biotec, Bergisch Gladbach, Germany)). To obtain HMDM, $CD14^+$ monocytes were cultured in RPMI 1640 medium (Sigma Aldrich) supplemented with 2 mmol/L L-glutamine, 100 IU/mL penicillin, 100 μg/mL streptomycin, and 10% heat inactivated FBS, all from Gibco Invitrogen Corporation (Paisley, UK), supplemented with 50 ng/mL recombinant M-CSF (Novakemi, Handen, Sweden) for three days. The HMDM phenotype was confirmed by analyzing the F4/80 (Abcam, Cambridge, UK) expression using flow cytometry (FACSCalibur, Becton Dickinson, Franklin Lakes, NJ). To obtain immature MDDC, $CD14^+$ monocytes were cultured at a density of 4×10^5 cells/mL at 37 °C in a humidified atmosphere containing 6% CO_2 in RPMI 1640 medium (Sigma Aldrich) supplemented with 2 mmol/L L-glutamine, 100 IU/mL penicillin, 100 μg/mL streptomycin (Gibco Invitrogen Corporation), 50 μM β-mercaptoethanol (KEBO-lab, Spånga, Sweden), 10% heat inactivated FCS (HyClone SH30071.03, Thermo Scientific, Waltham, MA) and supplemented with IL-4 (800 IU/mL) and GM-CSF (550 IU/mL) (Biosource International, Camarillo, CA). After three days, half of the culture medium was exchanged with fresh medium supplemented with IL-4 (800 IU/mL) and GM-CSF (550 IU/mL). After 6 days, the cells were analyzed by flow cytometry (FACSCalibur, Becton Dickinson) using fluorescein isothiocyanate (FITC) – or phycoerythrin (PE) – conjugated mouse monoclonal antibodies (MoAbs) against the cell surface molecules CD1a (Coulter Corporation, Hialeah, FL), CD11c, CD14 and CD83 (BioLegend, San Diego, CA). The immature phenotype of the MDDC was confirmed with low CD83 expression (always below 10%), CD1a (>80%), CD11c (>80%), and CD14 (<10%) (Vallhov et al., 2007). The mean viability of the MDDC, as determined by trypan blue exclusion, was always above 95%. This work was approved by the local ethics committee at the Karolinska Institutet.

Mitochondrial function of HMDM. Mitochondrial function in macrophages was determined by using 3-(4,5-dimethyldiazol-2-yl)-2,5 diphenyl-tetrazolium bromide (MTT) (Sigma Aldrich) (Cory et al., 1991). A number of 1×10^5 $CD14^+$ monocytes were seeded into a 96-well plate and differentiated to HMDM as described in the previous section. Cells were exposed to CSNPs and nanomag®-D-spio at the indicated concentrations for 24 and 48 h. The concentrations are expressed as μg of total weight of particles (for CSNPs: core plus silica shell: for nanomag®-D-spio: solid content) per mL. After exposure, the supernatant was removed and cells were washed once with phosphate-buffered saline (PBS) (pH 7.4). 100 μL of MTT solution (0.5 mg/mL) was added and incubated for 3 h at 37 °C. Finally, 50 μL of dimethyl sulfoxide (DMSO) (Sigma Aldrich) was added to dissolve the formazan crystals. MTT conversion was quantified by measuring the absorbance at 570 nm using a spectrophotometer (Infinite F200, Tecan, Männedorf, Switzerland).

Cell viability of MDDC and HMDM. Immature MDDC were seeded at a density of 4×10^5 cells/mL in 24 well plates (Falcon Multiwell™, Becton Dickinson) and exposed to CSNPs and nanomag®-D-spio for 24 and 48 h at 37 °C in a humidified atmosphere containing 6% CO_2. Cell viability was assessed using Annexin V and propidium iodide (PI) staining (BD Biosciences Pharmingen, Franklin Lakes, NJ) according to the manufacturer's instruction, and assessed using flow cytometry (FACSCalibur, Becton Dickinson). PI^-/Annexin V^+ events defined early apoptosis whereas PI^+/Annexin V^+ events were counted as late apoptosis or secondary necrosis, and all events are summarized as cell death. Approximately 1×10^5 cells were stained and 1×10^4 cells were acquired and analyzed by flow cytometry. In addition, cell viability in HMDM and MDDC was assessed by trypan blue exclusion. HMDM and MDDC were exposed to CSNPs and nanomag-D-®-spio at given concentrations for 24 and 48 h and the percentage of viable and dead cells was calculated. Results are expressed as percent of cell viability, mean ± SD using cells from different healthy blood donors.

Cytokine release. Culture supernatants from HMDM and MDDC were harvested at 24 and 48 h after nanoparticle or LPS (L8274, *Escherichia coli*, serotype 026-BG, Sigma Aldrich) exposure at given concentrations, and were kept at −80 °C until cytokine analysis. For HMDM, IL-6 and TNF-α and for MDDC, IL-12 (p70) and TNF-α release was determined by ELISA (Mabtech, Nacka, Sweden) according to the manufacturer's instruction. The absorbance was measured at 405 nm using a spectrophotometer (Infinite F200, Tecan, Männedorf, Switzerland, or Multiskan Ascent, Thermo Scientific). Results are expressed as pg/mL of released cytokine. The detection limits for TNF-α, IL-6, and IL-12 were 8 pg/mL, 4 pg/mL, and 5 pg/mL, respectively.

Cellular internalization studies. Internalization of CSNPs and nanomag®-D-spio was assessed by TEM analysis. HMDM and MDDC were exposed to 50 μg/mL of nanoparticles. After 2 or 24 h, cells were washed three times with PBS, fixed with a 0.2 M sodium cacodylate buffer containing 3% glutaraldehyde, pelleted and sucked up into a capillary tube (Leica Microsystems, Wetzlar, Germany). Fixed cells were post-fixed in 2% osmium tetroxide in 0.1 M sodium cacodylate buffer for 30 min, dehydrated through a graded ethanol series followed by acetone, and embedded in Epon resin (Fluka, Sigma Aldrich). Ultrathin sections were contrasted with 2% uranyl acetate and lead citrate (Reynolds, 1963) before observation in a Zeiss 900 TEM (Carl Zeiss MicroImaging GmbH, München, Germany) at 80 kV.

Inductively coupled plasma-mass spectrometry (ICP-MS). For quantification of cellular internalization of nanoparticles we measured cellular uptake of iron. Approximately 5×10^6 HMDM and MDDC were exposed to 50 μg/mL of nanoparticles for 2 or 24 h. The cells were then washed with PBS, counted and centrifuged at 200 g for 5 min. Cell pellets were kept at −80 °C until analysis. Measurement of

cellular iron content was performed using ICP-MS (Kippler et al., 2009a, 2009b) (Agilent 7500ce, Agilent Technologies, Tokyo, Japan) with a collision/reaction cell system, autosampler (Cetac ASX-510), and a quartz MicroMst nebulizer. The ICP-MS was operated at 1550 W with a reflected power of <5 W. For quality control (QC) purpose we used reference material (NIST1643c, Trace Elements in Water, National Institute of Standards and Technology, Gaithersburg, MD) with a certified value of 106.9 ± 3.0 μg/L. We obtained an average of 114.8 μg/L (n = 13). The limit of detection was 0.70 μg/L, calculated as 3 SD (n = 37). For some experiments, we used the Agilent 7700x (Agilent Technologies). Using the same reference material as above, we obtained an average of 127.83 μg/L (n = 6). The limit of detection was 0.235 μg/L, calculated as 3 SD (n = 12). Results are expressed as % of added iron concentration per 1000 cells, adjusted to control. To study whether the uptake process is active, HMDM were preincubated for 30 min with 10 μg/ml cytochalasin D (Sigma Aldrich) prior to nanoparticle exposure and ICP-MS analysis. Cell viability was >95% (trypan blue exclusion) when cells were cultured with cytochalasin D alone for 30 min followed by 24 h incubation.

Statistics. Differences between groups were evaluated using paired, two-tailed *t*-test or Tukey *post-hoc* test following one way ANOVA using GraphPad Prism version 5.02 for Windows (GraphPad Software, San Diego, CA). The level of significance for rejecting the null hypothesis of zero treatment effect was $p = 0.05$.

Results

Characterization of the nanoparticles

TEM was used to characterize the size and morphology of the CSNPs and nanomag®-D-spio nanoparticles. Hereafter the CSNPs are referred to as CSNPs 30 nm, 50 nm, 70 nm, and 120 nm, an approximation from the mean diameter presented in Table 1. In Fig. 1, the spherical shape, the core–shell architecture and the non-agglomerated character of CSNPs 30 nm (A), 50 nm (B), 120 nm (C) and 70 nm (D) are displayed. The TEM micrographs of nanomag®-D-spio (Figs. 1E–F) exhibit a cluster-like morphology with a high size polydispersity of clusters, characteristic for dextran-coated iron oxide nanoparticles. It should be pointed out that nanomag®-D-spio 20 and nanomag®-D-spio 50 refers to the cluster average sizes of 20 nm and 50 nm, respectively, as specified by the supplier.

The hydrodynamic size of the CSNPs and nanomag®-D-spio was measured in DI water and after incubation in RPMI 1640 cell culture media at 37 °C for 0 h, 2 h, 24 h and 48 h (Table 1). The hydrodynamic diameter of the CSNPs increased after incubation in cell culture media, compared to the diameter measured in DI water, whereas the hydrodynamic sizes of nanomag®-D-spio samples remained similar in the two dispersion media. This was probably due to the aging of the samples and subsequent instability of the clusters (Stromberg et al., 2007) which is also reflected in the observed formation of chain like structures, as seen in Figs. 1E–F. The hydrodynamic diameter of CSNP-30 nm particles appeared to increase more after incubation in cell culture media when compared to the larger particles with similar surface coating (Table 1); however, it should be noted that the dose of particles for these studies was based on mass. For a given mass, the effective surface area for CSNP-30 is approximately 1.6 and 3.6 times greater than for CSNP-50 and CSNP-130, respectively. The presence of a larger number of CSNP-30 with a larger total surface area may influence the interaction of the particles with its surroundings and could explain the increase in the hydrodynamic size upon incubation in cell culture medium containing fetal calf serum. Previous studies have shown that particle size influences the binding of proteins to the nanoparticle surface (Lundqvist et al., 2008).

The surface charge on CSNPs and nanomag®-D-spio was evaluated in DI water in the pH range of 4 to 9 (Fig. 2). CSNPs exhibited typical charge distribution of silica surface, and were negatively charged in the pH range of the current investigation, reaching −22 mV at physiological pH. Nanomag®-D-spio showed a small positive charge below pH 6.3 turning to a slightly negative charge above that, exhibiting surface potential of approximately −3 mV at physiological pH. These observations are consistent with earlier reports on dextran-coated nanoparticles exhibiting a surface charge of −1.5 mV at pH 7 (Vigor et al., 2010) while silica-coated iron oxide particles were found to have a surface charge of −25 mV at the same pH (Walczyk et al., 2010).

Magnetic properties of CSNPs and nanomag®-D-spio

VSM was used to assess the magnetic properties of the CSNPs and nanomag®-D-spio (Fig. 3). The superparamagnetic character of the core nanoparticles with a value of saturation magnetization (M_s) of 42.9 (±4.1) emu/g (expressed as emu per unit weight of Fe) is retained by the CSNPs when the silica thickness increases. The normalized M_s, values (expressed as emu per unit weight of CSNPs sample) are 20.7 emu/g, 9 emu/g, 4.1 emu/g and 0.5 emu/g for the CSNP samples with sizes of 30 nm, 50 nm, 70 nm and 120 nm corresponding to silica layer thicknesses of 6.5 nm, 17.4 nm, 23 nm and 51.5 nm respectively. The nanomag®-D-spio also exhibits superparamagnetic behavior with normalized values of M_s of 54 (±1.2) emu/g (expressed as emu per unit weight of Fe) (Fig. 3, inset).

Relaxivity studies were performed on the CSNPs and nanomag®-D-spio nanoparticles (Table 2). Previously reported values of commercially available T_2 contrast agents Resovist® (Qin et al., 2007; Geraldes and Laurent, 2009) and Feridex® (Josephson et al., 1988) were used for comparison. The r_2/r_1 ratios at 20 MHz of the CSNPs are higher than r_2/r_1 ratios for the commercially available

Table 1
DLS measurements of CSNPs and nanomag®-D-spio.

Particles	Mean hydrodynamic diameter (nm)[a]				
	DI water (25 °C)	RPMI medium (37 °C)			
		0 h	2 h	24 h	48 h
CSNPs[b] 27.1 ± 1.57 nm	44.4 ± 4.0	122.4 ± 17.9	122.4 ± 9.6	141.8 ± 1.0	153 ± 6.5
CSNPs[b] 48.8 ± 2.9 nm	125.6 ± 5.6	147.2 ± 5.6	156.7 ± 6.4	172.8 ± 14.9	172.8 ± 14.9
CSNPs[b] 68.5 ± 4.8 nm	140.3 ± 2.05	168.5 ± 7.4	172.8 ± 14.9	164.17 ± 0.04	164.2 ± 0.04
CSNPs[b] 117 ± 4.7 nm	145.5 ± 6.4	195.1 ± 8.6	200.1 ± 17.3	195.1 ± 8.6	200.1 ± 17.3
Nanomag®-D-spio 20	87.1 ± 3.6	83.1 ± 1.8	82.9 ± 3.6	93.6 ± 4.1	93.1 ± 3.3
Nanomag®-D-spio 50	73.4 ± 0.01	91.9 ± 11.3	77.03 ± 3.1	80.9 ± 3.6	80.9 ± 3.6

The DLS values are measured for CSNPs with different sizes and the commercial iron oxide-based MR contrast agents nanomag®-D-spio in distilled water (pH = 7) at 25 °C and in RPMI 1640 cell culture medium (pH = 7.4) supplemented with 10% FCS at 37 °C.
[a] Measurements were performed on a colloidal suspension of particles, mean ± SD, n = 3.
[b] Diameter of the CSNPs obtained from TEM micrographs measurements, mean ± SD, n ≥ 300.

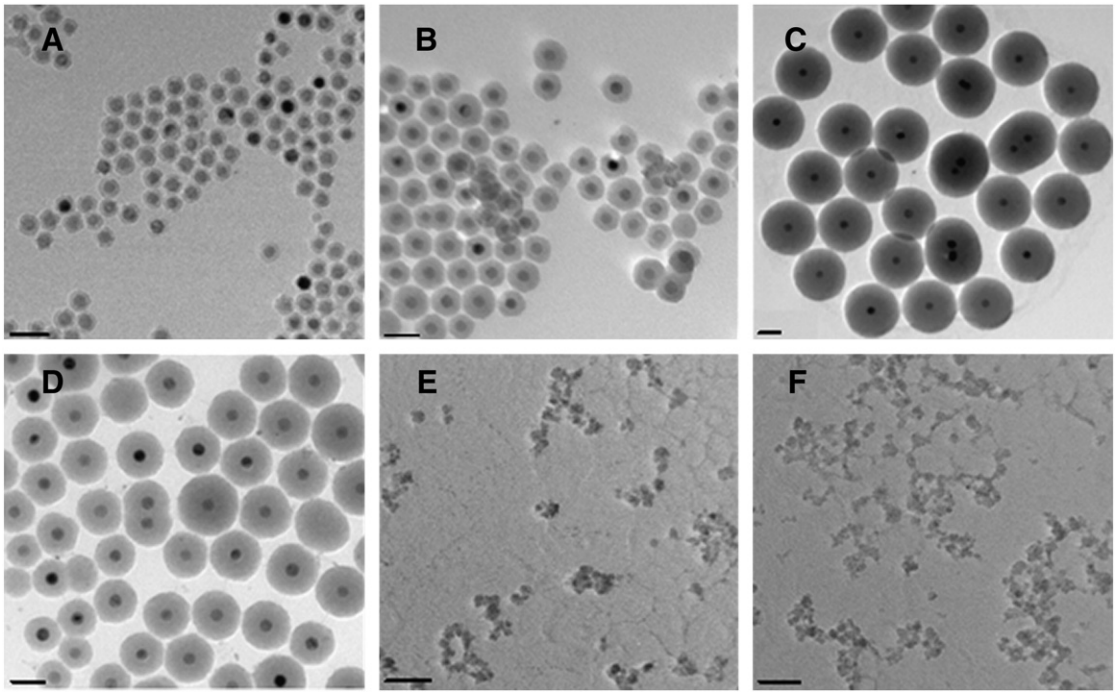

Fig. 1. Visualization of CSNPs and nanomag®-D-spio. TEM images of CSNPs (A–C) with average particle sizes of 30 nm (A), 50 nm (B), 120 nm (C) and 70 nm (D), nanomag®-D-spio 20 (E) and nanomag®-D-spio 50 (F). The scale bars are 50 nm in all TEM micrographs.

contrast agents Resovist®, Feridex®, nanomag®-D-spio 20 and nanomag®-D-spio 50.

Effect of CSNPs and nanomag®-D-spio on cell viability

In order to investigate the biocompatibility of the CSNPs and nanomag®-D-spio, mitochondrial function of HMDM exposed to the nanoparticles was determined using the MTT assay (Fig. 4). No interference between the MTT and the nanoparticles was observed (Suppl. Fig. S1). The mitochondrial function of HMDM exposed to the different nanoparticles for 24 and 48 h was not affected, although a trend for a decrease in mitochondrial function was observed at a concentration of 100 μg/mL for all sizes of CSNPs (Figs. 4A–C). None of the nanomag®-D-spio samples caused a decrease in the mitochondrial function of HMDM (Figs. 4D–E).

Cell death of MDDC after nanoparticle exposure was assessed using Annexin V and PI staining (Vallhov et al., 2007) (Fig. 5). There was a dose-dependent increase of cell death in MDDC after 24 and 48 h exposure to CSNPs of smaller sizes (30 nm and 50 nm), compared to MDDC cultured in medium alone. The exposure to CSNPs 120 nm, or the nanomag®-D-spio 20 and 50, however, did not induce cell death after 24 or 48 h exposure. To verify if the toxicity in MDDC is a size-dependent effect of the silica-coated iron oxide nanoparticles or due to the different synthesis procedures, we produced particles with an average size of 70 nm (CSNPs 70 nm) by the Stöber method (Stöber et al., 1968), the same method that was used to generate the CSNPs 120 nm, and incubated these particles with MDDC. No toxicity was induced when MDDC were exposed to the CSNPs 70 nm (Fig. 5C). Hence, a size-dependent effect seems apparent.

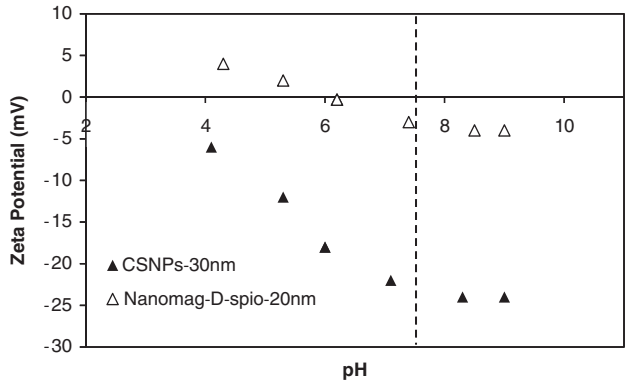

Fig. 2. Zeta potential measurement of CSNPs and nanomag®-D-spio. The zeta potential was evaluated for silica-coated CSNPs (30 nm) and dextran-coated nanomag®-D-spio 50 nm in DI water in the pH range of 4 to 9. The dotted line indicates the physiological pH.

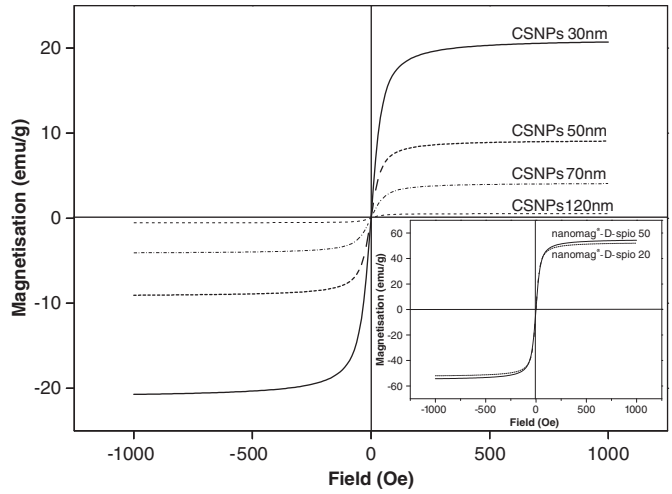

Fig. 3. Magnetic properties of the CSNPs and nanomag®-D-spio. Magnetic measurements performed by VSM on the CSNPs of average size of 30 nm (__), 50 nm (- -), 70 nm (-·-·-) and 120 nm (- -). The inset represents the saturation magnetizations for the nanomag®-D-spio 20 (▬) and nanomag®-D-spio 50 (__).

Table 2
Relaxivity properties of CSNPs and nanomag®-D-spio.

Particles	Coating material/thickness (nm)	$r_1(s^{-1}\ mM^{-1})$[a]		$r_2(s^{-1}\ mM^{-1})$[a]		r_2/r_1	
		20 MHz	60 MHz	20 MHz	60 MHz	20 MHz	60 MHz
CSNPs 30 nm	SiO_2/6.5[b]	7.4 ± 0.3	1.7 ± 0.1	106.6 ± 3.2	123.2 ± 0.7	14.4	72.5
CSNPs 50 nm	SiO_2/17.4[b]	1.4 ± 0.1	0.7 ± 0.03	85.9 ± 2.6	100.3 ± 0.9	61.4	143.3
CSNPs 70 nm	SiO_2/23[b]	0.8 ± 0.02	0.5 ± 0.02	70.8 ± 0.8	87.2 ± 0.9	88.5	174.4
CSNPs 120 nm	SiO_2/51.5[b]	0.9 ± 0.04	0.5 ± 0.02	38.9 ± 0.7	46.9 ± 0.9	43.2	93.8
Nanomag®-D-spio 20	Dextran	27.6 ± 0.1	8.9 ± 0.08	165.5 ± 1.0	160.4 ± 1.0	6	18
Nanomag®-D-spio 50	Dextran	27.9 ± 0.1	9.5 ± 0.1	142.2 ± 1.1	142.1 ± 0.9	5.1	14.9
Resovist	Carboxy-dextran	24.9	10.9	177	190	7.1	17.4
Feridex	Dextran	40	NA	160	NA	4	NA

The relaxivity values of CSNPs with different thicknesses of the silica layer compared to the commercial iron oxide based MR contrast agents Resovist®, Feridex® and nanomag®-D-spio. The values for the commercial iron oxide based MR contrast agents nanomag®-D-spio are measured values while for Resovist® and Feridex® the values are reported in literature (Qin et al., 2007; Stromberg et al., 2007; Geraldes and Laurent, 2009). Relaxivity values are measured at 20 MHz (0.47 T) and 60 MHz (1.41 T) in water (37 °C). NA: not applicable.
[a] Results presented as mean ± SD, n = 3.
[b] SiO_2 shell thickness was measured from TEM micrographs.

To ensure that the differences in cell viability of HMDM and MDDC exposed to CSNPs were not due to the different viability methods used in both cell types, trypan blue exclusion was used. Trypan blue exclusion (Suppl. Fig. S2) confirmed the data obtained by MTT assay and AnnexinV/PI staining, respectively. Thus, HMDM were not affected upon exposure to any of the tested particles (Suppl. Figs. S2A–B),

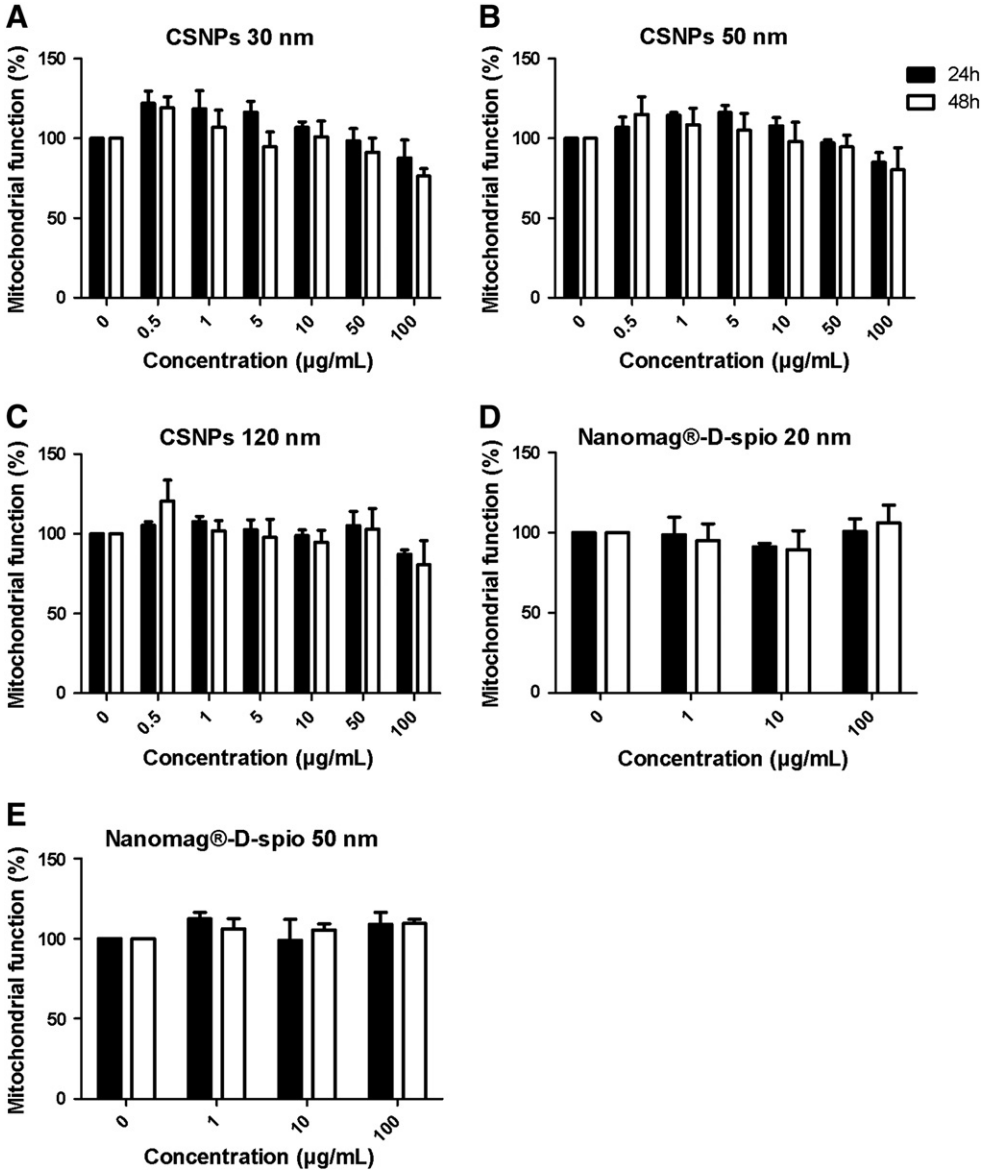

Fig. 4. Mitochondrial function in HMDM. HMDM were exposed to various concentrations of CSNPs (A–C) or nanomag®-D-spio (D–E) for 24 h (black bar) and 48 h (white bar). Mitochondrial function was assessed using the MTT assay. Results are presented as percent mitochondrial function (mean ± SD) from three independent experiments using cells from different healthy blood donors. No statistically significant differences were detected using one way ANOVA.

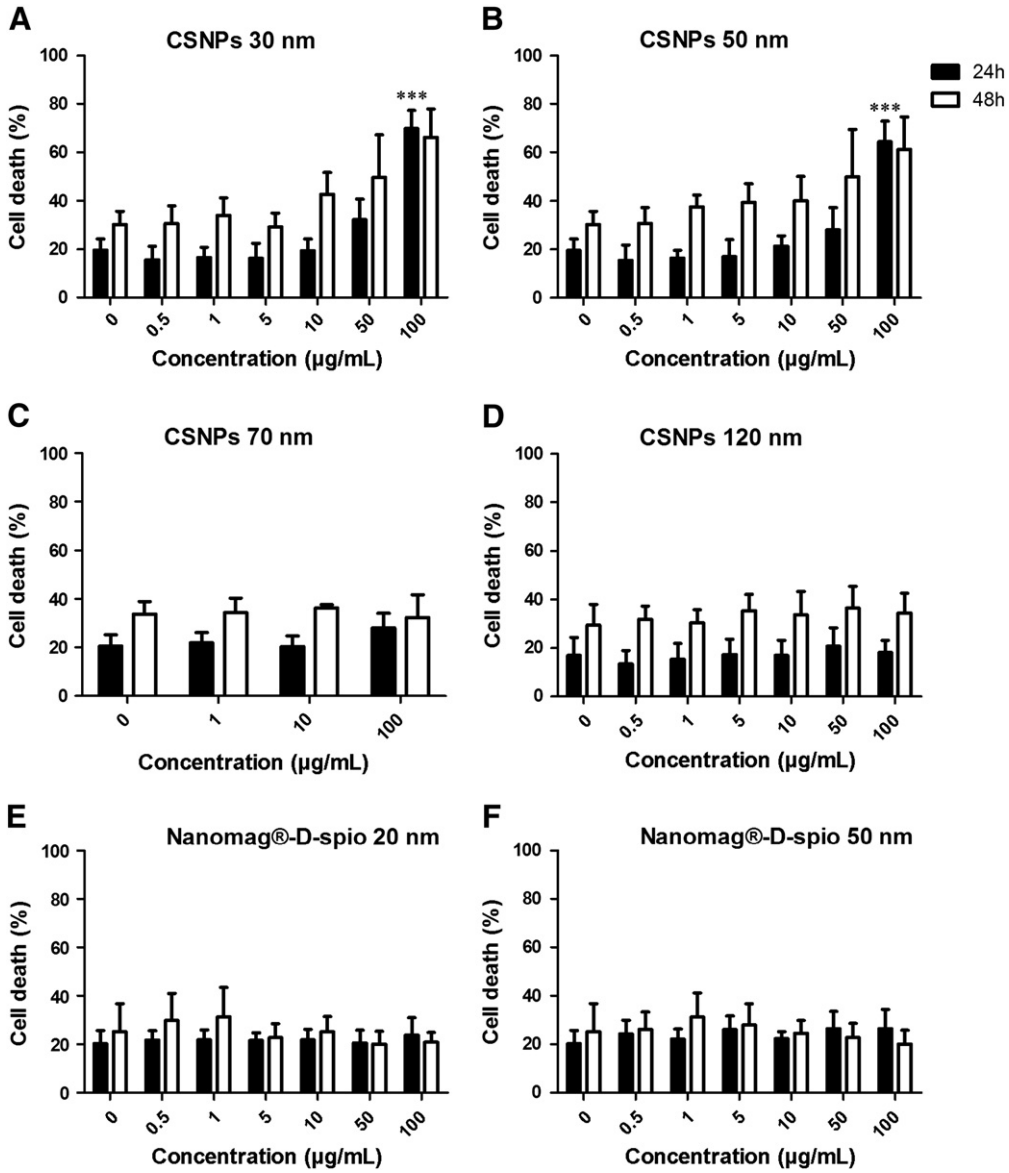

Fig. 5. Cell viability in MDDC. MDDC were exposed to various concentrations of CSNPs (A–D) or nanomag®-D-spio (E–F) for 24 h (black bar) and 48 h (white bar). Cell viability was assessed by flow cytometry using the AnnexinV/PI assay. Results are presented as percent cell death (sum of apoptosis and necrosis, mean ± SD) from three to five independent experiments using cells from different healthy blood donors. Statistical analysis was performed using Tukey *post-hoc* test following one way ANOVA (***$p<0.001$).

whereas the cell viability of MDDC was decreased upon exposure to CSNPs 30 nm and 50 nm, but not after exposure to the CSNPs 70 and 120 nm particles (Suppl. Figs. S2C–D). Taken together, MDDC appear to be more vulnerable than HMDM to the effects of the smaller CSNPs. The similarly small nanomag®-D-spio were non-toxic to MDDC.

Cytokine release

Cytokine release was studied as an immune modulatory end-point in HMDM and MDDC after exposure to CSNPs and nanomag®-D-spio. Production of TNF-α, a pro-inflammatory cytokine known to be released from activated HMDM and MDDC, was not induced after 24 h (Suppl. Fig. S3) or 48 h of nanoparticle exposure (Fig. 6). LPS induced a significant release of TNF-α in both cell types, as expected (Fig. 6). Additionally, no induction of the pro-inflammatory cytokines IL-6 (for HMDM) (Suppl. Figs. S4 and S5) or IL-12 (p70) (for MDDC) was detected (Suppl. Figs. S6 and S7) upon incubation of cells with CSNPs or nanomag®-D-spio for 24 or 48 h.

Internalization of iron oxide nanoparticles

Internalization of the CSNPs and nanomag®-D-spio by HMDM (Fig. 7) and MDDC (Fig. 8) was visualized using TEM. We noted that the CSNPs (50 µg/mL) of all three sizes (30, 50 and 120 nm) were taken up after 2 h by HMDM (Figs. 7A–C) and MDDC (Figs. 8A–C). In both cell types, the particles were predominantly located in membrane-enclosed vesicles, indicating the involvement of an active uptake mechanism such as endocytosis. The CSNPs frequently appeared as single (monodispersed) particles. In contrast, the cellular internalization of nanomag®-D-spio was sparse when assessed after 2 h of incubation (Suppl. Fig. S8). However, internalization of the nanomag®-D-spio (20 and 50 nm) by HMDM (Figs. 7E–F) and MDDC (Figs. 8D–E) could be observed when the incubation time was extended to 24 h.

To quantify the uptake of nanoparticles, we utilized ICP-MS. The experiments confirmed that the uptake of CSNPs by HMDM and MDDC was higher when compared to nanomag®-D-spio (Figs. 9A–B). The differences between CSNPs and nanomag®-D-spio were thus

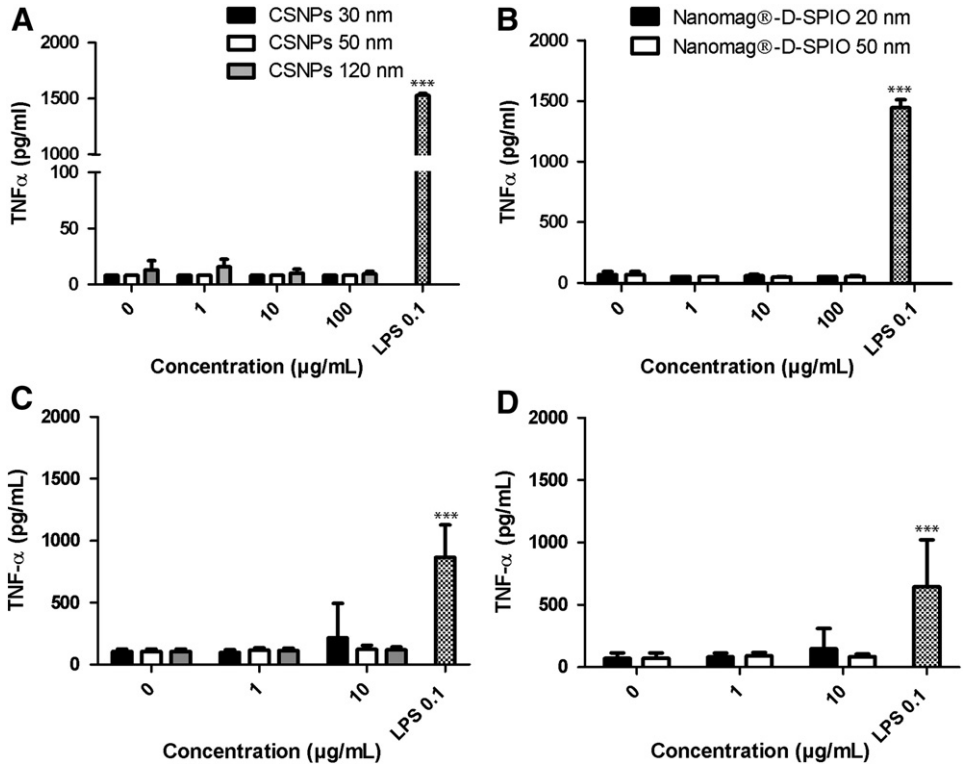

Fig. 6. TNF-α secretion in HMDM and MDDC. Cytokine release was assessed using ELISA. HMDM (A–B) and MDDC (C–D) were exposed to various concentrations of CSNPs (A and C) or nanomag®-D-spio (B and D) for 48 h. LPS was used as a positive control. Results are presented as TNF-α release (pg/mL) (mean ± SD) from three independent experiments using cells from different healthy blood donors. Statistical analysis was performed using Tukey *post-hoc* test following one way ANOVA (**$p<0.01$, ***$p<0.001$).

statistically significant for HMDM and a similar trend was noted for MDDC, but this did not reach statistical significance. The uptake of CSNPs and nanomag®-D-spio was time-dependent, as higher uptake could be observed after 24 h compared to 2 h (Suppl. Fig. S9). Our studies also provided some indication that the uptake of larger (120 nm) CSNPs was greater than for the smaller CSNPs at 2 h of exposure, but the degree of uptake overall was low at this time-point. On the other hand, when cellular uptake was determined at 24 h, there were no significant differences in the degree of uptake between the different sizes of CSNPs (Figs. 9A–B). Moreover, pretreatment of HMDM with cytochalasin D, which prevents actin cytoskeleton reorganization (Wodnicka et al., 1992), significantly diminished the uptake of CSNPs by HMDM (Fig. 9A), indicating the involvement of an active, endocytic internalization process. A similar trend albeit not statistically significant was seen for MDDC (Fig. 9B).

Discussion

In the present study, the magnetic properties, biocompatibility and efficiency of cellular internalization of novel silica-coated CSNPs compared to commercial dextran-coated nanomag®-D-spio were evaluated in primary human macrophages and dendritic cells. The CSNPs revealed superior magnetic properties, and displayed a higher efficiency of cellular uptake when compared to the nanomag®-D-spio. The CSNPs were non-toxic to macrophages at all sizes tested whereas the smaller nanoparticles (30 nm and 50 nm) displayed dose-dependent cytotoxicity towards dendritic cells. The nanomag®-D-spio were non-toxic to both cell types.

For the complete physical characterization of iron oxide-based contrast agents, a set of three measurements is required in order to predict their performance as MRI applications: relaxometry, magnetization and light scattering (Koenig et al., 2002). The monodispersed, nonaggregated CSNPs were proven to perform well on all measurements. MR signal intensity depends on the intrinsic longitudinal (r_1) and transverse (r_2) relaxivities, finally determining the imaging contrast. Iron oxide based contrast agents have emerged as T_2 contrast agents, as they exhibit r_2 values much higher than r_1 values which reflect in high r_2/r_1 ratios (Mornet et al., 2004; Patel et al., 2010). The nanomag®-D-spio nanoparticles exhibit similar r_2/r_1 ratios as commercial MRI contrast agents (Resovist® and Feridex®) due to the similar sized magnetic core (less than 10 nm), similar coating materials and comparable hydrodynamic diameters of the clusters. In the case of CSNPs the increase of the silica layer thickness will impede the interactions between the magnetic core and the surrounding solvent protons in both 20 MHz and 60 MHz fields. This causes a strong reduction of the longitudinal relaxation r_1, while the effect on the transverse relaxation r_2 is much smaller (Roch et al., 2005). As a result, the r_2/r_1 ratios of all average sizes of CSNPs are substantially higher than the commercial MRI contrast agents, indicating a much better performance as T_2 contrast agents. Therefore the CSNPs are sufficiently magnetically responsive for medical imaging or cell tracking applications.

Previous studies showed that large iron oxide nanoparticles (80 nm) are quickly internalized by macrophages and have a shorter blood circulation time (Weissleder et al., 1989) when compared to small iron oxide nanoparticles (30 nm) (Bourrinet et al., 2006), suggesting that particle size plays a major role for internalization by cells of the reticulo-endothelial system (Metz et al., 2004; Raynal et al., 2004). However, our *in vitro* studies revealed a comparable degree of internalization of all sizes of CSNPs (from 30 to 120 nm) in HMDM and MDDC, when particle uptake was monitored at 24 h. The surfaces of nanoparticles are modified when particles are placed in a biological medium, such as human plasma, which may affect the subsequent particle–cell interactions (Cederwall et al., 2007; Aggarwal et al., 2009; Walczyk et al., 2010). Indeed, a recent study has shown that negatively charged poly(acrylic acid)-conjugated gold nanoparticles bind to and induce unfolding of fibrinogen, which promotes interaction with the integrin receptor, Mac-1 (Deng et al.,

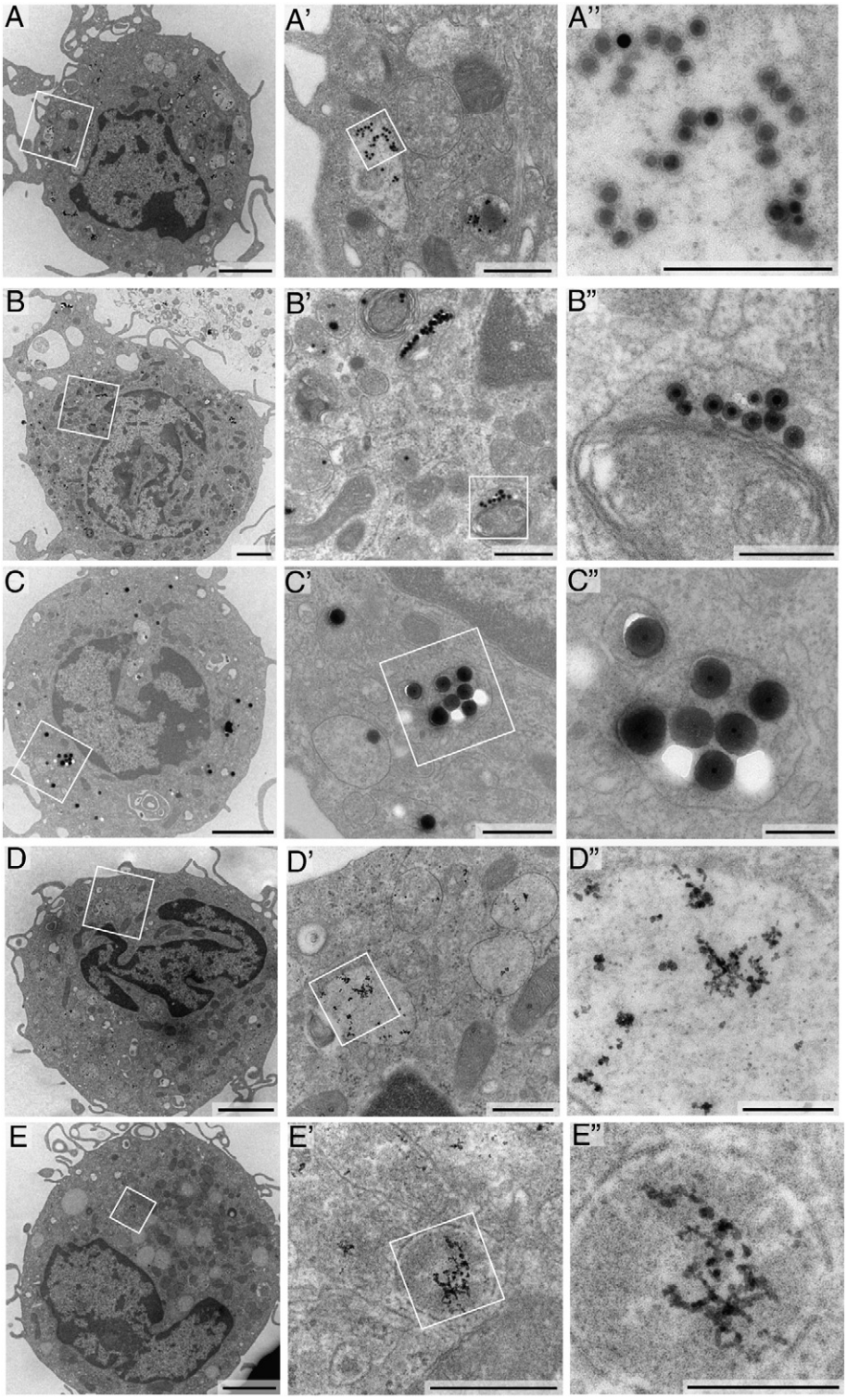

Fig. 7. Internalization of CSNPs and nanomag®-D-spio by HMDM. Micrographs of HMDM exposed to 50 μg/mL of CSNPs 30 nm (A–A″), 50 nm (B–B″) or 120 nm (C–C″) for 2 h and HMDM exposed to 50 μg/mL of nanomag®-D-spio 20 (D–D″) and nanomag®-D-spio 50 (E–E″) for 24 h. X′ and X″ represent enlargements of the white quadrant in X or X′, respectively. Scale bars: A–E: 2 μM; A′–E′: 500 nm; A″–E″: 200 nm.

2011). DLS data suggest that the hydrodynamic sizes of the silica-coated particles increased in cell culture medium supplemented with fetal calf serum, while the dextran-coated particle sizes were more stable under these conditions. However, the DLS method has its limitations regarding complex mixed samples (Walczyk et al., 2010). Our results suggest that the uptake of SPIONs by primary human immune-competent cells is determined, at least in part, by the nature of the surface coating, as the silica-coated particles were taken up to a greater extent when compared to dextran-coated particles, as determined by ICP-MS. These differences in surface coating, and in surface charge, could in turn affect the nature of the protein corona, and cellular uptake.

In the present study, the cell viability of HMDM was not affected by CSNPs or nanomag®-D-spio nanoparticles, while a dose-dependent

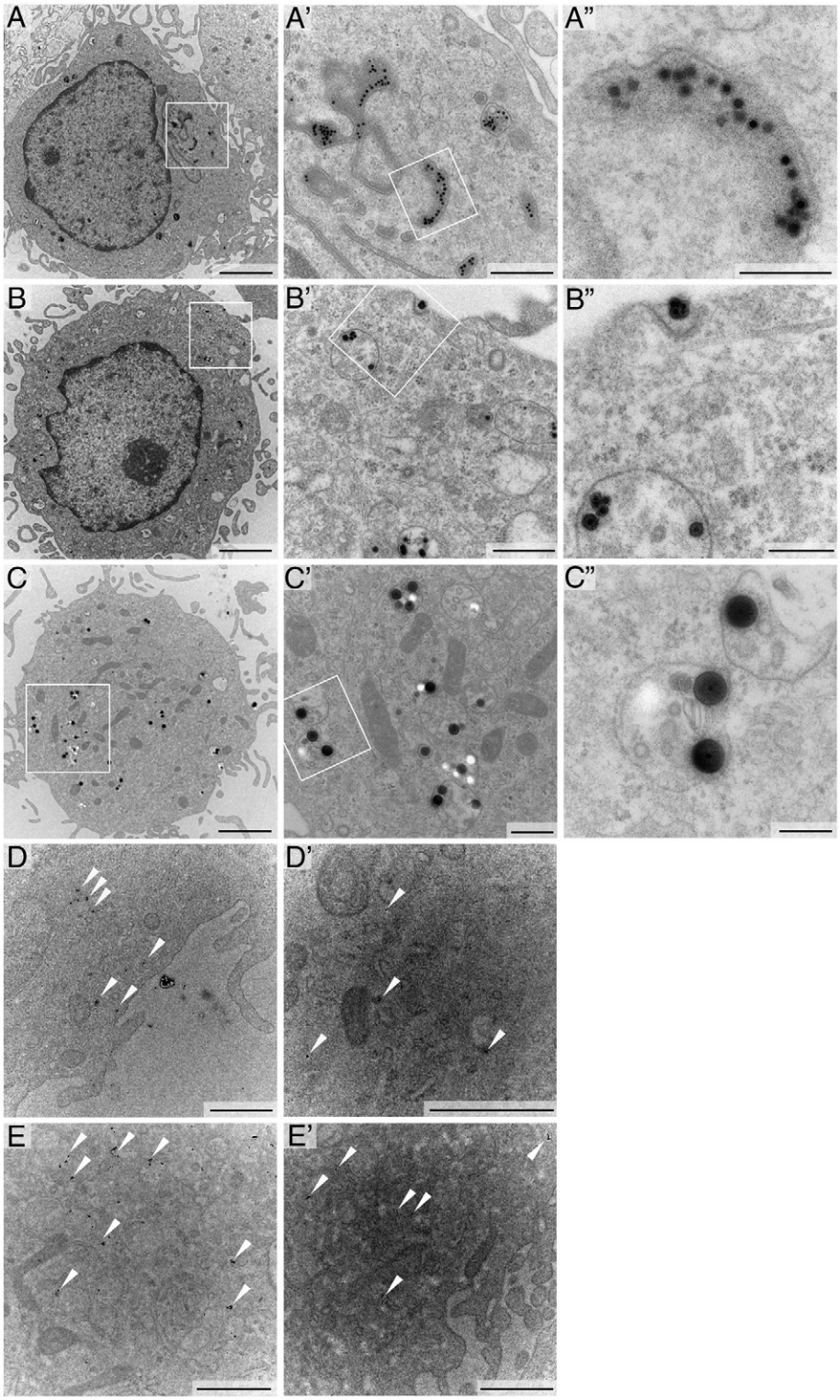

Fig. 8. Internalization of CSNPs and nanomag®-D-spio by MDDC. Micrographs of MDDC exposed to 50 μg/mL of CSNPs 30 nm (A–A″), CSNPs 50 nm (B–B″) or CSNPs 120 nm (C–C″) for 2 h. Micrographs of uncontrasted sections of MDDC exposed to nanomag®-D-spio 20 (D–D′) and nanomag®-D-spio 50 (E–E′) for 24 h. Some nanoparticles in D–E′ are highlighted with arrowheads. X′ and X″ represent enlargements of the white quadrant in X or X′, respectively. Scale bars: A–C: 2 μm; A′–C′: 500 nm; A″–C″: 200 nm; D–E′: 1 μm.

decrease in viability was seen in MDDC exposed to smaller (30 nm and 50 nm) CSNPs, but not when the cells were exposed to 120 nm CSNPs. The observed difference in toxicity between HMDM and MDDC was not due to the use of different toxicity assays. We questioned whether differences in the synthesis method could account for the cell viability results, but this was also ruled out. Specifically, we reasoned that the decreased cell viability of MDDC caused by the 30 nm and 50 nm CSNPs could be related to residual amounts of the solvent (ethanol) since the silica coating of CSNPs 30 nm and 50 nm was applied according to a different procedure compared to CSNPs 70 nm and 120 nm (see Materials and methods). However, control experiments conducted with a range of concentrations of ethanol alone showed that this was unlikely to be the case (Suppl. Fig. S10). Therefore, our conclusion is that size-dependent effects on cell

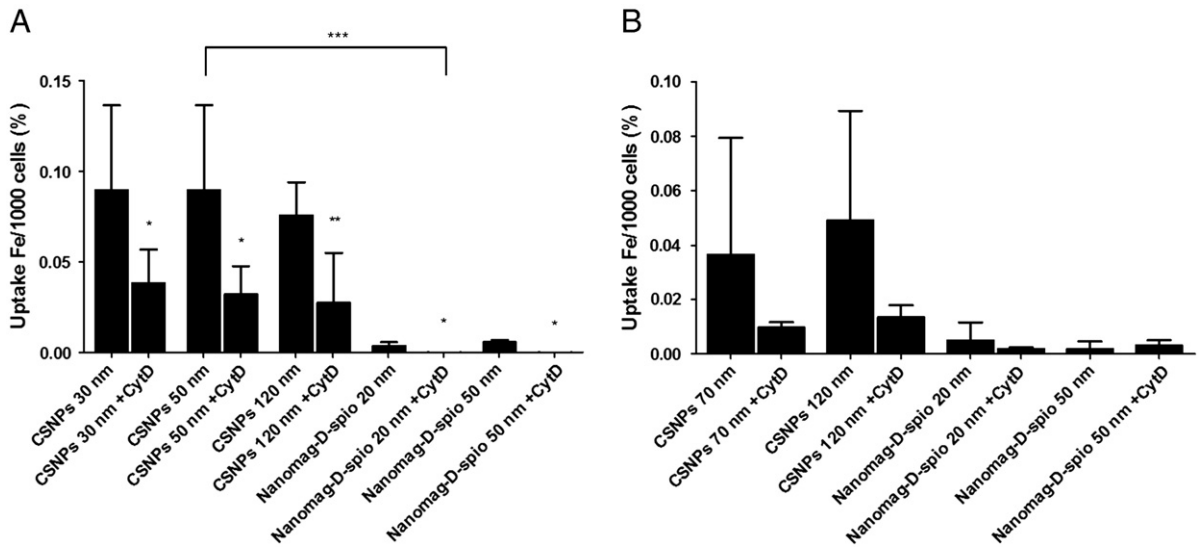

Fig. 9. Quantification of iron oxide uptake by HMDM and MDDC. Cellular internalization of CSNPs and nanomag®-D-spio was quantified by ICP-MS determination of iron. HMDM (A) and MDDC (B) were exposed to 50 μg/mL iron oxide nanoparticles for 24 h. Uptake of CSNPs was examined in the presence or absence of cytochalasin D (Cyt D). Results are presented as % of added iron concentration per 1000 cells (mean ± SD) adjusted to control, from three to six independent experiments, using cells from different healthy blood donors. Statistical analysis of the differences in uptake in samples treated versus not treated with Cyt D was performed using Student's *t*-test (*$p<0.05$, **$p<0.01$). The difference in the degree of cellular uptake between the two types of SPIONs (CSNPs versus nanomag®-D-spio) was evaluated using Tukey *post-hoc* test following one way ANOVA. The difference was significant for HMDM (***$p<0.001$) but not for MDDC.

viability are seen for MDDC but not for HMDM. The fact that MDDC may be more vulnerable was suggested in previous studies, showing that HMDM were unaffected by mesoporous silica particles (Witasp et al., 2009a), whereas MDDC were affected in a dose- and size-dependent manner (Vallhov et al., 2007).

The doses used in the present *in vitro* study (up to 100 μg/mL) are in the range of doses commonly applied for *in vitro* testing of engineered nanoparticles including SPIONs (Kunzmann et al., 2011; Mahmoudi et al., 2011). In order to compare these doses to the doses achieved in human subjects upon administration of SPIONs, we calculated the iron content in PBS following the addition of SPIONs of different sizes and different surface coatings (silica versus dextran) using ICP-MS. Based on these calculations, the doses of iron for SPIONs added at a concentration of 100 μg/mL are approximately 23, 9.9, 0.75, 21, and 17 μg/mL for CSNP-30 nm, CSNP-50 nm, CSNP-120 nm, nanomag®-D-spio-20 nm, and nanomag®-D-spio-50 nm, respectively. For comparison, the mean ± SD peak serum iron concentration in healthy adult volunteers who received a dose of Feridex I.V.® (ferumoxide) of 0.56 mg of Fe/kg bodyweight (i.e. the highest approved dose for this particular SPION) was 5.5 ± 0.6 μg/mL (http://www.drugs.com/pro/feridex.html). In other words, the concentrations of iron in our *in vitro* studies are comparable to, or exceed, the levels of iron achieved *in vivo* in human subjects. This gives us confidence that the current *in vitro* results are relevant to the human situation.

MRI requires high concentrations of contrast agents to achieve a clear imaging signal (Qin et al., 2007). The nanomag®-D-spio nanoparticles used in this study were not effectively internalized in HMDM and MDDC, despite their performance in recent *in vivo* MRI studies (Oghabian et al., 2010). The differences in coating materials and consequently different surface charges of the nanomag®-D-spio and CSNP may partly explain the different internalization efficiencies reported here. Due to their high surface charge, CSNPs are predicted to interact with proteins electrostatically forming H-bonds or to interact strongly with the carboxyl groups of the proteins. Dextran-coated particles, on the other hand, will interact mainly via H-bond formation (Vigor et al., 2010) and are thus predicted to exhibit less surface-protein interactions. Further studies are warranted to study the protein binding to the different SPIONs.

The efficient internalization of CSNP by immune-competent cells is of considerable importance, as it offers the potential of using these CSNPs for *in vivo* cell tracking. Cell tracking can be applied to follow the migration of monocytes/macrophages to the site of inflammation to clarify the role of immune cells in e.g. neuronal diseases (Zelivyanskaya et al., 2003). In addition, Bierry et al. (2010) reported that SPIONs could be used to depict knee infection in an experimental rabbit model, and Truijers et al. (2009) have shown that SPIONs could be utilized for non-invasive imaging of macrophage infiltration in abdominal aortic aneurysms in patients. Furthermore, recent work shows that iron oxide-labeled cells can be directed to specific anatomic sites by so-called magnetic resonance targeting (MRT) (Riegler et al., 2010). With respect to dendritic cells, successful MRI tracking of dendritic cells was demonstrated in cancer patients and could perhaps be exploited for monitoring of cellular therapy (de Vries et al., 2005).

Conclusions

We have compared the cytotoxicity and cellular uptake by primary human immune-competent cells of two types of SPIONs: *de novo* synthesized silica-coated iron oxide nanoparticles of different sizes (ranging from 30 nm to 120 nm) and commercially available dextran-coated iron oxide nanoparticles (nanomag®-D-spio) with average cluster sizes of 20 nm and 50 nm. The degree of uptake by macrophages was shown to be greater for silica-coated particles than for the dextran-coated particles. The observed differences could be related to the differences in surface charge of the coating materials which, in turn, could affect the binding of proteins to these particles.

Overall, due to the physical characteristics (monodispersed, nonaggregated, and with a tuneable silica shell), magnetic properties (superparamagnetic and high r_2/r_1 ratio) and generally low toxicity of the novel CSNPs, with no effects on pro-inflammatory cytokine secretion by primary human immune cells, these materials appear to be suitable candidates for bioimaging applications such as MRI and cellular tracking where the tracking of macrophages or dendritic cells is desirable (monitoring of inflammation or monitoring cell migration during cellular therapy). Further studies on the biodistribution and biocompatibility of these materials *in vivo* are needed.

Conflict of interest statement

The authors declare that there are no conflicts of interest.

Acknowledgments

The authors are supported by the Seventh Framework Programme of the European Commission (EC-FP7-NANOMMUNE-Grant Agreement No. 214281), the ARC Program 05/10-335 of the French Community of Belgium, the Knut and Alice Wallenberg Foundation, the Swedish Research Council for Working Life and Social Research, and the Swedish Research Council. We thank Liliane Diener, Swiss Federal Laboratories for Materials Testing and Research, and Margareta Grandér and Brita Palm, Karolinska Institutet, for excellent technical assistance with TEM and ICP-MS, respectively. We are also grateful to Dr. Helen Vallhov, Karolinska Institutet, for excellent technical assistance and advice regarding the culture of MDDC.

Appendix A. Supplementary data

Supplementary data to this article can be found online at doi:10.1016/j.taap.2011.03.011.

References

Aggarwal, P., Hall, J.B., McLeland, C.B., Dobrovolskaia, M.A., McNeil, S.E., 2009. Nanoparticle interaction with plasma proteins as it relates to particle biodistribution, biocompatibility and therapeutic efficacy. Adv. Drug Deliv. Rev. 61, 428–437.

Banchereau, J., Steinman, R.M., 1998. Dendritic cells and the control of immunity. Nature 392, 245–252.

Barrera, C., Herrera, A.P., Rinaldi, C., 2009. Colloidal dispersions of monodisperse magnetite nanoparticles modified with poly(ethylene glycol). J. Colloid Interface Sci. 329, 107–113.

Bierry, G., Jehl, F., Neuville, A., Lefevre, S., Robert, P., Kremer, S., Dietemann, J.L., 2010. MRI of macrophages in infectious knee synovitis. AJR Am. J. Roentgenol. 194, W521–W526.

Bourrinet, P., Bengele, H.H., Bonnemain, B., Dencausse, A., Idee, J.M., Jacobs, P.M., Lewis, J.M., 2006. Preclinical safety and pharmacokinetic profile of ferumoxtran-10, an ultrasmall superparamagnetic iron oxide magnetic resonance contrast agent. Investig. Radiol. 41, 313–324.

Bumb, A., Brechbiel, M.W., Choyke, P.L., Fugger, L., Eggeman, A., Prabhakaran, D., Hutchinson, J., Dobson, P.J., 2008. Synthesis and characterization of ultra-small superparamagnetic iron oxide nanoparticles thinly coated with silica. Nanotechnology 19, 335601.

Bumb, A., Regino, C.A., Perkins, M.R., Bernardo, M., Ogawa, M., Fugger, L., Choyke, P.L., Dobson, P.J., Brechbiel, M.W., 2010. Preparation and characterization of a magnetic and optical dual-modality molecular probe. Nanotechnology 21, 175704.

Cederwall, T., Lynch, I., Foy, M., Berggard, T., Donnelly, S.C., Cagney, G., Linse, S., Dawson, K.A., 2007. Detailed identification of plasma proteins adsorbed on copolymer nanoparticles. Angew. Chem. Int. Ed Engl. 46, 5754–5756.

Cory, A.H., Owen, T.C., Barltrop, J.A., Cory, J.G., 1991. Use of an aqueous soluble tetrazolium/formazan assay for cell growth assays in culture. Cancer Commun. 3, 207–212.

de Vries, I.J., Lesterhuis, W.J., Barentsz, J.O., Verdijk, P., van Krieken, J.H., Boerman, O.C., Oyen, W.J., Bonenkamp, J.J., Boezeman, J.B., Adema, G.J., Bulte, J.W., Scheenen, T.W., Punt, C.J., Heerschap, A., Figdor, C.G., 2005. Magnetic resonance tracking of dendritic cells in melanoma patients for monitoring of cellular therapy. Nat. Biotechnol. 23, 1407–1413.

Deng, Y.-H., Wang, C.-C., Hu, J.-H., Yang, W.-L., Fu, S.-K., 2005. Investigation of formation of silica-coated magnetite nanoparticles via sol–gel approach. Colloid Surf. Physicochem. Eng Asp. 262, 87–93.

Deng, Z.J., Liang, M., Monteiro, M., Toth, I., Minchin, R.F., 2011. Nanoparticle-induced unfolding of fibrinogen promotes Mac-1 receptor activation and inflammation. Nat. Nanotechnol. 6, 39–44.

Dobrovolskaia, M.A., McNeil, S.E., 2007. Immunological properties of engineered nanomaterials. Nat. Nanotechnol. 2, 469–478.

Dutz, S., Andrä, W., Hergt, R., Müller, R., Oestreich, C., Schmidt, C., Töpfer, J., Zeisberger, M., Bellemann, M.E., 2007. Influence of dextran coating on the magnetic behaviour of iron oxide nanoparticles. J. Magn. Magn. Mater. 311, 51–54.

Fleige, G., Seeberger, F., Laux, D., Kresse, M., Taupitz, M., Pilgrimm, H., Zimmer, C., 2002. *In vitro* characterization of two different ultrasmall iron oxide particles for magnetic resonance cell tracking. Investig. Radiol. 37, 482–488.

Flogel, U., Ding, Z., Hardung, H., Jander, S., Reichmann, G., Jacoby, C., Schubert, R., Schrader, J., 2008. *In vivo* monitoring of inflammation after cardiac and cerebral ischemia by fluorine magnetic resonance imaging. Circulation 118, 140–148.

Geraldes, C., Laurent, S., 2009. Classification and basic properties of contrast agents for magnetic resonance imaging. Contrast Media Mol. Imaging 4, 1–23.

Gordon, S., Taylor, P.R., 2005. Monocyte and macrophage heterogeneity. Nat. Rev. Immunol. 5, 953–964.

Hamm, B., Staks, T., Taupitz, M., Maibauer, R., Speidel, A., Huppertz, A., Frenzel, T., Lawaczeck, R., Wolf, K.J., Lange, L., 1994. Contrast-enhanced MR imaging of liver and spleen: first experience in humans with a new superparamagnetic iron oxide. J. Magn. Reson. Imaging 4, 659–668.

Im, S.H., Herricks, T., Lee, Y.T., Xia, Y., 2005. Synthesis and characterization of monodisperse silica colloids loaded with superparamagnetic iron oxide nanoparticles. Chem. Phys. Lett. 401, 19–23.

Josephson, L., Lewis, J., Jacobs, P., Hahn, P.F., Stark, D.D., 1988. The effects of iron oxides on proton relaxivity. Magn. Reson. Imaging 6, 647–653.

Kippler, M., Goessler, W., Nermell, B., Ekstrom, E.C., Lonnerdal, B., El Arifeen, S., Vahter, M., 2009a. Factors influencing intestinal cadmium uptake in pregnant Bangladeshi women—a prospective cohort study. Environ. Res. 109, 914–921.

Kippler, M., Lonnerdal, B., Goessler, W., Ekstrom, E.C., Arifeen, S.E., Vahter, M., 2009b. Cadmium interacts with the transport of essential micronutrients in the mammary gland — a study in rural Bangladeshi women. Toxicology 257, 64–69.

Kobukai, S., Baheza, R., Cobb, J.G., Virostko, J., Xie, J., Gillman, A., Koktysh, D., Kerns, D., Does, M., Gore, J.C., Pham, W., 2010. Magnetic nanoparticles for imaging dendritic cells. Magn. Reson. Med. 63, 1383–1390.

Koenig, S.H., Kellar, K.E., Fujii, D.K., Gunther, W.H.H., Briley-Saebo, K., Spiller, M., 2002. Three types of physical measurements needed to characterize iron oxide nanoparticles for MRI and MRA: magnetization, relaxometry, and light scattering. Acad. Radiol. 9, S5–S10.

Kunzmann, A., Andersson, B., Thurnherr, T., Krug, H., Scheynius, A., Fadeel, B., 2011. Toxicology of engineered nanomaterials: focus on biocompatibility, biodistribution and biodegradation. Biochim. Biophys. Acta 1810, 361–373.

Laurent, S., Boutry, S., Mahieu, I., Vander Elst, L., Muller, R.N., 2009. Iron oxide based MR contrast agents: from chemistry to cell labeling. Curr. Med. Chem. 16, 4712–4727.

Lin, W., Huang, Y.W., Zhou, X.D., Ma, Y., 2006. *In vitro* toxicity of silica nanoparticles in human lung cancer cells. Toxicol. Appl. Pharmacol. 217, 252–259.

Liong, M., Lu, J., Kovochich, M., Xia, T., Ruehm, S.G., Nel, A.E., Tamanoi, F., Zink, J.I., 2008. Multifunctional inorganic nanoparticles for imaging, targeting, and drug delivery. ACS Nano 2, 889–896.

Lu, Y., Yin, Y., Mayers, B.T., Xia, Y., 2002. Modifying the surface properties of superparamagnetic iron oxide nanoparticles through a sol–gel approach. Nano Lett. 2, 183–186.

Lu, C.-W., Hung, Y., Hsiao, J.-K., Yao, M., Chung, T.-H., Lin, Y.-S., Wu, S.-H., Hsu, S.-C., Liu, H.-M., Mou, C.-Y., Yang, C.-S., Huang, D.-M., Chen, Y.-C., 2007. Bifunctional magnetic silica nanoparticles for highly efficient human stem cell labelling. Nano Lett. 7, 149–154.

Lundqvist, M., Stigler, J., Elia, G., Lynch, I., Cedervall, T., Dawson, K.A., 2008. Nanoparticle size and surface properties determine the protein corona with possible implications for biological impacts. Proc. Natl Acad. Sci. U. S. A. 105, 14265–14270.

Mahmoudi, M., Sahraian, M.A., Shokrgozar, M.A., Laurent, S., 2011. Superparamagnetic iron oxide nanoparticles: promises for diagnosis and treatment of multiple sclerosis. ACS Chem. Neurosci 2, 118–140.

Metz, S., Bonaterra, G., Rudelius, M., Settles, M., Rummeny, E.J., Daldrup-Link, H.E., 2004. Capacity of human monocytes to phagocytose approved iron oxide MR contrast agents *in vitro*. Eur. Radiol. 14, 1851–1858.

Mornet, S., Vasseur, S., Grasset, F., Duguet, E., 2004. Magnetic nanoparticle design for medical diagnosis and therapy. J. Mater. Chem. 14, 2161–2175.

Narita, A., Nakab, K., Chujo, Y., 2009. Facile control of silica shell layer thickness on hydrophilic iron oxide nanoparticles via reverse micelle method. Colloid Surf. Physicochem. Eng. Asp. 336, 46–56.

Oghabian, M.A., Gharehaghaji, N., Amirmohseni, S., Khoei, S., Guiti, M., 2010. Detection sensitivity of lymph nodes of various sizes using USPIO nanoparticles in magnetic resonance imaging. Nanomedicine 6, 496–499.

Patel, D., Kell, A., Simard, B., Deng, J., Xiang, B., Lin, H.Y., Gruwel, M., Tian, G., 2010. Cu(2+)-labeled, SPION loaded porous silica nanoparticles for cell labeling and multifunctional imaging probes. Biomaterials 31, 2866–2873.

Qin, J., Laurent, S., Jo, Y.S., Roch, A., Mikhaylova, M., Bhujwalla, Z.M., Muller, R.N., Muhammed, M., 2007. A high-performance magnetic resonance imaging T-2 contrast agent. Adv. Mater. 19, 1874–1878.

Rao, K.S., El-Hami, K., Kodaki, T., Matsushige, K., Makino, K., 2005. A novel method for synthesis of silica nanoparticles. J. Colloid Interface Sci. 289, 125–131.

Raynal, I., Prigent, P., Peyramaure, S., Najid, A., Rebuzzi, C., Corot, C., 2004. Macrophage endocytosis of superparamagnetic iron oxide nanoparticles: mechanisms and comparison of ferumoxides and ferumoxtran-10. Investig. Radiol. 39, 56–63.

Reimer, P., Balzer, T., 2003. Ferucarbotran (Resovist): a new clinically approved RES-specific contrast agent for contrast-enhanced MRI of the liver: properties, clinical development, and applications. Eur. Radiol. 13, 1266–1276.

Reynolds, E.S., 1963. The use of lead citrate at high pH as an electron-opaque stain in electron microscopy. J. Cell Biol. 17, 208–212.

Riegler, J., Wells, J.A., Kyrtatos, P.G., Price, A.N., Pankhurst, Q.A., Lythgoe, M.F., 2010. Targeted magnetic delivery and tracking of cells using a magnetic resonance imaging system. Biomaterials 31, 5366–5371.

Riehemann, K., Schneider, S.W., Luger, T.A., Godin, B., Ferrari, M., Fuchs, H., 2009. Nanomedicine-challenge and perspectives. Angew. Chem. Int. Ed Engl. 48, 872–897.

Roch, A., Gossuin, Y., Muller, R.N., Gillis, P., 2005. Superparamagnetic colloid suspensions: water magnetic relaxation and clustering. J. Magn. Magn. Mater. 293, 532–539.

Salgueiriño-Maceira, V., Correa-Duarte, M.A., 2007. Increasing the complexity of magnetic core/shell structured nanocomposites for biological applications. Adv. Mater. 19, 4131–4144.

Santra, S., Tapec, R., Theodoropoulou, N., Dobson, J., Hebard, A., Tan, W., 2001. Synthesis and characterization of silica-coated iron oxide nanoparticles in microemulsion: the effect of nonionic surfactants. Langmuir 17, 2900–2906.

Shvedova, A.A., Kagan, V.E., Fadeel, B., 2010. Close encounters of the small kind: adverse effects of man-made materials interfacing with the nano-cosmos of biological systems. Annu. Rev. Pharmacol. Toxicol. 50, 63–88.

Stromberg, M., Gunnarsson, K., Valizadeh, S., Svedlindh, P., Stromme, M., 2007. Aging phenomena in ferrofluids suitable for magnetic biosensor applications. J. Appl. Phys. 101.

Stöber, W., Fink, A., Bohn, E., 1968. Controlled growth of monodisperse silica spheres in the micron size range. J. Colloid Interface Sci. 26, 62–69.

Truijers, M., Fütterer, J.J., Takahashi, S., Heesakkers, R.A., Blankensteijn, J.D., Barentsz, J.O., 2009. *In vivo* imaging of the aneurysm wall with MRI and a macrophage-specific contrast agent. AJR Am. J. Roentgenol. 193, W437–W441.

Valable, S., Barbier, E.L., Bernaudin, M., Roussel, S., Segebarth, C., Petit, E., Remy, C., 2008. *In vivo* MRI tracking of exogenous monocytes/macrophages targeting brain tumors in a rat model of glioma. Neuroimage 40, 973–983.

Vallhov, H., Qin, J., Johansson, S.M., Ahlborg, N., Muhammed, M.A., Scheynius, A., Gabrielsson, S., 2006. The importance of an endotoxin-free environment during the production of nanoparticles used in medical applications. Nano Lett. 6, 1682–1686.

Vallhov, H., Gabrielsson, S., Stromme, M., Scheynius, A., Garcia-Bennett, A.E., 2007. Mesoporous silica particles induce size dependent effects on human dendritic cells. Nano Lett. 7, 3576–3582.

Veiseh, O., Gunn, J.W., Zhang, M., 2009. Design and fabrication of magnetic nanoparticles for targeted drug delivery and imaging. Adv. Drug Deliv. Rev. 62, 284–304.

Vigor, K.L., Kyrtatos, P.G., Minogue, S., Al-Jamal, K.T., Kogelberg, H., Tolner, B., Kostarelos, K., Begent, R.H., Pankhurst, Q.A., Lythgoe, M.F., Chester, K.A., 2010. Nanoparticles functionalized with recombinant single chain Fv antibody fragments (scFv) for the magnetic resonance imaging of cancer cells. Biomaterials 31, 1307–1315.

Walczyk, D., Bombelli, F.B., Monopoli, M.P., Lynch, I., Dawson, K.A., 2010. What the cell "sees" in bionanoscience. J. Am. Chem. Soc. 132, 5761–5768.

Weissleder, R., Stark, D.D., Engelstad, B.L., Bacon, B.R., Compton, C.C., White, D.L., Jacobs, P., Lewis, J., 1989. Superparamagnetic iron oxide: pharmacokinetics and toxicity. AJR Am. J. Roentgenol. 152, 167–173.

Witasp, E., Kupferschmidt, N., Bengtsson, L., Hultenby, K., Smedman, C., Paulie, S., Garcia-Bennett, A.E., Fadeel, B., 2009a. Efficient internalization of mesoporous silica particles of different sizes by primary human macrophages without impairment of macrophage clearance of apoptotic or antibody-opsonized target cells. Toxicol. Appl. Pharmacol. 239, 306–319.

Witasp, E., Shvedova, A.A., Kagan, V.E., Fadeel, B., 2009b. Single-walled carbon nanotubes impair human macrophage engulfment of apoptotic cell corpses. Inhal. Toxicol. 21, 131–136.

Wodnicka, M., Pierzchalska, M., Bereiter-Hahn, J., Kajstura, J., 1992. Comparative study on effects of cytochalasins B and D on F-actin content in different cell lines and different culture conditions. Folia Histochem. Cytobiol. 30, 107–111.

Vogt, C., Laurent, S., Bridot, J.-L., Muller, R., Toprak, M.S., Muhammed, M., 2010. High quality and tuneable silica shell–magnetic core nanoparticles. J. Nanopart. Res. 12, 1137–1147.

Yi, D.K., Lee, S.S., Papaefthymiou, G.C., Ying, J.Y., 2006. Nanoparticle architectures templated by SiO_2/Fe_2O_3 nanocomposites. Chem. Mater. 18, 614–619.

Yi, D.K., Selvan, S.T., Lee, S.S., Papaefthymiou, G.C., Kundaliya, D., Ying, J.Y., 2005. Silica-coated nanocomposites of magnetic nanoparticles and quantum dots. J. Am. Chem. Soc. 127, 4990–4991.

Zelivyanskaya, M.L., Nelson, J.A., Poluektova, L., Uberti, M., Mellon, M., Gendelman, H.E., Boska, M.D., 2003. Tracking superparamagnetic iron oxide labeled monocytes in brain by high-field magnetic resonance imaging. J. Neurosci. Res. 73, 284–295.

Zhang, M., Cushing, B.L., O'Connor, C.J., 2008. Synthesis and characterization of monodisperse ultra-thin silica-coated magnetic nanoparticles. Nanotechnology 19 085601/085601-085601/085605.